Power System Technology
ISSN:1000-3673

Received: 10-01-2024 Revised: 02-02-2024 Accepted: 04-03-2024

An Algorithm for a Space-Vector Pulse Width Modulation with a Hybrid Switching Sequence for a Three-Level Neutral Point Clamped Voltage Source Inverter

M. M. Dudkin[1], A. N. Shishkov[2], V. K. Le[3]

[1]Professor, Department of Electric Drives, Mechatronics and Electromechanics, South Ural State University (National Research University), Chelyabinsk, Russian Federation.
[2]Associate Professor, Department of Electrical Equipment and Industrial Electronics, Moscow Polytechnic University, Moscow, Russian Federation.
[3]Postgraduate Student, Department of Electrical Equipment and Industrial Electronics, Moscow Polytechnic University, Moscow, Russian Federation.
Email: [1]dudkinmm@susu.ru, [2]shan1982@mail.ru, [3]canhlv.mta@gmail.com

Abstract: This paper proposes a new algorithm for a space-vector pulse width modulation (SVPWM) with a hybrid switching sequence (SS) designed to control a three-level (3L) neutral point clamped (NPC) voltage source inverter (VSI). Based on the advantages of five-stage and seven-stage SS, we designed a hybrid SS to improve four key parameters in the system: inverter output current quality, neutral point (NP) and common-mode (CM) voltage levels, and switching losses of power switches. The proposed algorithm flexibly regulates meeting the four criteria depending on the system operating conditions by changing the regulation coefficient. The paper obtained an approximate dependence to determine the optimal regulation coefficient for any values of the inverter modulation coefficient when operating jointly with an active-inductive load. The effectiveness of the proposed algorithm is confirmed by computer simulation in the *MatLab+Simulink* environment, as well as the results of experimental studies. The paper presents the experimental dependences of static state spaces, including the distortion coefficient of higher current harmonics at the inverter output, the maximum error of the NP voltage, the number of switching pairs of power switches, and the pulse duty factor of CM voltage, depending on the inverter modulation coefficient and the regulation coefficient of the hybrid SS. The results showed that in the algorithm for a SVPWM with a hybrid SS, the number of switchings of power switches is reduced by an average of 13.5 % while maintaining the NP voltage balance and the quality of the curve at the inverter output at an acceptable level, close to a seven-stage SS (the deviations do not exceed 0.5 % and 0.2 %, respectively). The average CM voltage coefficient decreased by no more than 4.5 %. The indicators improve the energy saving, the weight-size parameters, and the operational reliability of the 3L NPC VSI. The application area of the algorithm is much wider and includes the control of power switches of active front ends, grid converters for electricity storage systems, active power filters, and power conditioners.

Keywords: multi-level inverter, three-level neutral point clamped voltage source inverter, space-vector pulse width modulation, hybrid switching sequence, neutral point voltage, switching losses, common-mode voltage.

Power System Technology
ISSN:1000-3673

Received: 10-01-2024 Revised: 02-02-2024 Accepted: 04-03-2024

1. Introduction

In recent years, multilevel (ML) voltage source inverters (VSI) have been increasingly applied in the field of high-voltage alternating current electric drives [1, 2], as well as in devices to enhance the power quality in power supply systems [3]. Currently, numerous topologies of multilevel inverters have been proposed, among which the most popular are ML Neutral Point Clamped (NPC) VSI, Flying Capacitor ML VSI, Cascaded H-bridge ML VSI [4], and others. The topology with flying capacitors requires the use of a large number of high-capacity capacitors, leading to significant voltage imbalance issues the capacitors and, as a consequence, an increase in the size and cost of the device [5]. The cascaded ML VSI topology is close to achieving an ideal level as it is built on modular cells, allowing for easy power scaling, simultaneously increasing the output frequency and the quality of the ML VSI output voltage [6]. The only drawback of this topology is the complex power supply system for modular cells, requiring galvanic isolation. Despite the numerous proposed ML VSI topologies, interest in the research of three-level (3L) NPC VSI remains high to date [7]. This topology was proposed by Akira Nabae, Isao Takahashi, and Hirofumi Akagi in 1981 [8] and has found wide application in power electronics due to its relatively simple power scheme, low cost, and high energy efficiency [9]. Therefore, research and development in this area continue as there is a need for optimization and improvement of the characteristics and performance of this VSI topology.

Figure 1 presents a three-phase topology of a 3L NPC VSI. Each phase contains four power switches $S_{x1}…S_{x4}$ and two clamping diodes $D_{x1}…D_{x2}$ (x is the index of phase a, b, c). Two capacitors C_{d1} and C_{d2} connected in series in the DC link act as a voltage divider of the inverter power supply. If the voltage balance between the capacitors is maintained, the power supply voltage U_d is divided into three voltage levels: $-U_d/2$, 0, $+U_d/2$ [8]. Each phase at the inverter output takes one of three states: [P], [O], [N]. For phase state [P] (switches S_{x4}, S_{x3} are on) the phase voltage u_{x0} relative to point O is $+U_d/2$; for phase state [O] (switches S_{x3}, S_{x2} are on) u_{x0} is 0, and for phase state [N] (switches S_{x2}, S_{x1} are on) u_{x_0} is $-U_d/2$.

Currently, much attention is devoted to the control methods of 3L NPC VSI [10-14]. Among them, the space-vector PWM (SVPWM) algorithm has gained significant popularity for controlling these inverters [15-20]. Various versions of the SVPWM algorithm have been proposed in numerous publications in recent years, allowing improvement in one of the following tasks: enhancing the quality of the output voltage and current [15], improving the neutral point (NP) voltage balance [16, 17], reducing switching losses [18], and decreasing the level of common-mode (CM) voltage [19, 20]. However, a common drawback for such control strategies is the inability to simultaneously improve all characteristics, i.e., enhancing one characteristic leads to the deterioration of another and vice versa [21]. Therefore, the development of control algorithms for 3L NPC VSI to enhance their technical characteristics,

Power System Technology
ISSN:1000-3673
Received: 10-01-2024 Revised: 02-02-2024 Accepted: 04-03-2024

including energy efficiency, size and weight considerations, and operational reliability, remains a relevant task.

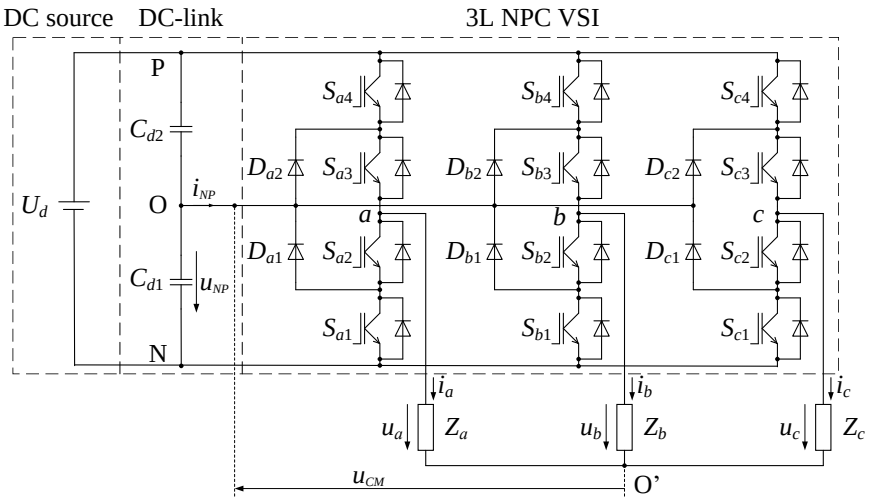

Fig. 1. Three-phase topology of a 3L NPC VSI

This work particularly focuses on crucial indicators of a three-level inverter system, such as the balance of the NP voltage in the DC link, switching losses, the quality of the output voltage and current, and the level of CM voltage.

As known, an imbalance in the NP voltage adversely affects the operation of the inverter and the load overall, potentially causing failures in both power switches and capacitors in the DC-link due to voltage surges and increased ripple levels [22]. Therefore, to enhance the operational reliability of the inverter, the voltage between the two capacitors in the DC-link of the 3L NPC VSI must be strictly controlled and equal to half the voltage of the power source U_d (see Fig. 1).

The switching loss indicator directly influences the efficiency of the inverter, which is particularly crucial for high-power converters (units, tens of megawatts). The quality of the output voltage and current affects power losses in the load from higher harmonics and also impacts the size and weight parameters of sinusoidal filters if applied to suppress high-frequency harmonics and overvoltages on the load due to the high rate of voltage change at the inverter output.

CM voltage is also an essential technical issue in a 3L NPC VSI. CM voltage is measured between point O of the power supply and the neutral point of the three-phase load O' (see Fig. 1). Most works [16, 17] optimizing the NP voltage ignore the CM voltage issue, although a high level of CM voltage can cause overvoltage in the motor winding insulation, increasing

Power System Technology
ISSN:1000-3673
Received: 10-01-2024 Revised: 02-02-2024 Accepted: 04-03-2024

electromagnetic interference and, consequently increasing the high-frequency current through the motor bearings, etc. [23].

Considering the above, the main goal of this work is to develop a new SVPWM algorithm with a hybrid switching sequence (SS) for controlling a 3L NPC VSI. This algorithm differs from known SVPWM algorithms by the capability of simultaneously achieving the four criteria mentioned above. This paper proposes a new algorithm for a SVPWM with a hybrid SS, which provides acceptable indicators for the four tasks. This method is based on the hybridization of a 7-stage SS and a 5-stage SS, hence a SVPWM with a hybrid SS. The 7-stage SS provides a high level of NP voltage balance and the high quality of the output current curve but leads to high CM voltage and major switching losses [24]. The 5-stage SS provides the opposite results [25]. Using the strengths of the 5-stage and 7-stage SS in the algorithm allowed us to achieve the following results: an acceptable quality of the output current curve; acceptable NP voltage balance; reduced switching losses compared to a 7-stage SS; and improved CM voltage compared to a 7-stage SS.

2. Algorithm of a space-vector PWM to control a 3L NPC VSI

The three-phase topology of a 3L NPC VSI has $3^3 = 27$ switching combinations for power switches corresponding to 19 basic voltage vectors (Fig. 2). The vector diagram is a regular hexagon consisting of six identical sectors I…VI, each of which is divided into four segments: 1 (*a*, *b*), 2, 3 (*a*, *b*), 4. Depending on the length of the vector, basic vectors are classified into 6 large vectors $\bar{U}_{L1}\ldots\bar{U}_{L6}$, 6 medium $\bar{U}_{M1}\ldots\bar{U}_{M6}$, 6 small $\bar{U}_{S1}\ldots\bar{U}_{S6}$ and zero $\bar{U}_0$ (19 in total). Small basic vectors can be formed from 12 combinations, of which 6 are *p*-type (without state [N]) and 6 are *n*-type (without state [P]).

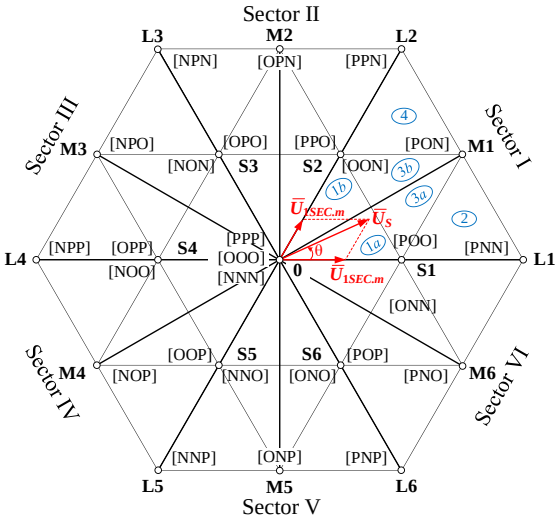

Fig. 2. Vector diagram for a 3L NPC VSI

Power System Technology
ISSN:1000-3673
Received: 10-01-2024 Revised: 02-02-2024 Accepted: 04-03-2024

The influence of basic vectors on the NP voltage balance is discussed in detail in [26]. Large basic and zero vectors do not affect the NP voltage. For medium vectors, the NP voltage can increase or decrease depending on the inverter operating conditions, but the influence of this vector is negligible. Small vectors significantly affect the NP voltage. In motor mode, *p*-type combinations increase the NP voltage, while *n*-type combinations have the opposite effect.

The influence of basic vectors on the CM voltage are summarized in Table 1 [22]. State combinations are divided into four groups corresponding to different CM voltage levels. The combinations from sectors III and IV are least often used when developing SVPWM-based algorithms, since they generate a high CM voltage.

At SVPWM, during one quantization period T_{PWM} the spatial voltage vector $\bar{U}_s$ is synthesized from the basic vectors located at the vertices of the triangle according to the "volt-second balance" principle [27]. Using segment 1*a* (sector I) as an example, basic vectors $\bar{U}_{S1}$, $\bar{U}_{S2}$ and $\bar{U}_0$ can be selected to synthesize the spatial vector $\bar{U}_s$ (see. Fig. 2). According to the principle of the nearest three vectors, the spatial vector $\bar{U}_s$ at SVPWM can be written as:

$$\begin{cases} \bar{U}_s = \gamma_1 \bar{U}_{S1} + \gamma_2 \bar{U}_{S2} + \gamma_3 \bar{U}_0; \\ \gamma_1 + \gamma_2 + \gamma_3 = 1. \end{cases} \tag{1}$$

Here $\gamma_1 = t_1/T_{PWM}$; $\gamma_2 = t_2/T_{PWM}$ and $\gamma_3 = t_3/T_{PWM}$ are the relative durations of switching the basic vectors $\bar{U}_{S1}$, $\bar{U}_{S2}$ and $\bar{U}_0$, respectively, and t_1, t_2, and t_3 are their absolute values.

Table 1. The influence of basic vectors on the CM voltage

Sector	Basic vector	CM voltage
I	$\bar{U}_{M1}$[PON], $\bar{U}_{M2}$ [OPN],$\bar{U}_{M3}$[NPO], $\bar{U}_{M4}$[NOP], $\bar{U}_{M5}$[ONP], $\bar{U}_{M6}$[PNO], $\bar{U}_0$[OOO]	0
II	$\bar{U}_{L1}$[PNN], $\bar{U}_{L3}$[NPN], $\bar{U}_{L5}$[NNP], $\bar{U}_{S2n}$[OON], $\bar{U}_{S4n}$[NOO], $\bar{U}_{S6n}$[ONO]	$-U_d/6$
	$\bar{U}_{L2}$[PPN], $\bar{U}_{L4}$[NPP], $\bar{U}_{L6}$[PNP], $\bar{U}_{S1p}$[POO], $\bar{U}_{S3p}$[OPO], $\bar{U}_{S5p}$[OOP]	$+U_d/6$
III	$\bar{U}_{S1n}$[ONN], $\bar{U}_{S3n}$[NON], $\bar{U}_{S5n}$[NNO]	$-U_d/3$
	$\bar{U}_{S2p}$[PPO], $\bar{U}_{S4p}$[OPP], $\bar{U}_{S6p}$[POP]	$+U_d/3$
IV	$\bar{U}_0$[NNN]	$-U_d/2$

Power System Technology
ISSN:1000-3673
Received: 10-01-2024 Revised: 02-02-2024 Accepted: 04-03-2024

	$\bar{U}_0$ [PPP]	$+U_d/2$

7-stage (Table 2) and 5-stage (Table 3) switching sequences are most widespread to control a 3L NPC VSI [7].

Table 2. The 7-stage SS for sector I

Segment 1*a*	$\bar{U}_{S1p}$	$\bar{U}_0$	$\bar{U}_{S2n}$	$\bar{U}_{S1n}$	$\bar{U}_{S2n}$	$\bar{U}_0$	$\bar{U}_{S1p}$
	[POO]	[OOO]	[OON]	[ONN]	[OON]	[OOO]	[POO]
Segment 1*b*	$\bar{U}_{S2n}$	$\bar{U}_0$	$\bar{U}_{S1p}$	$\bar{U}_{S2p}$	$\bar{U}_{S1p}$	$\bar{U}_0$	$\bar{U}_{S2n}$
	[OON]	[OOO]	[POO]	[PPO]	[POO]	[OOO]	[OON]
Segment *2*	$\bar{U}_{S1p}$	$\bar{U}_{M1}$	$\bar{U}_{L1}$	$\bar{U}_{S1n}$	$\bar{U}_{L1}$	$\bar{U}_{M1}$	$\bar{U}_{S1p}$
	[POO]	[PON]	[PNN]	[ONN]	[PNN]	[PON]	[POO]
Segment 3*a*	$\bar{U}_{S1p}$	$\bar{U}_{M1}$	$\bar{U}_{S2n}$	$\bar{U}_{S1n}$	$\bar{U}_{S2n}$	$\bar{U}_{M1}$	$\bar{U}_{S1p}$
	[POO]	[PON]	[OON]	[ONN]	[OON]	[PON]	[POO]
Segment 3*b*	$\bar{U}_{S2n}$	$\bar{U}_{M1}$	$\bar{U}_{S1p}$	$\bar{U}_{S2p}$	$\bar{U}_{S1p}$	$\bar{U}_{M1}$	$\bar{U}_{S2n}$
	[OON]	[PON]	[POO]	[PPO]	[POO]	[PON]	[OON]
Segment 4	$\bar{U}_{S2n}$	$\bar{U}_{M1}$	$\bar{U}_{L2}$	$\bar{U}_{S2p}$	$\bar{U}_{L2}$	$\bar{U}_{M1}$	$\bar{U}_{S2n}$
	[OON]	[PON]	[PPN]	[PPO]	[PPN]	[PON]	[OON]

Table 3. The 5-stage SS for sector I

Segment 1*a*	$\bar{U}_{S1p}$	$\bar{U}_0$	$\bar{U}_{S2n}$	$\bar{U}_0$	$\bar{U}_{S1p}$
	[POO]	[OOO]	[OON]	[OOO]	[POO]
Segment 1*b*	$\bar{U}_{S2n}$	$\bar{U}_0$	$\bar{U}_{S1p}$	$\bar{U}_0$	$\bar{U}_{S2n}$
	[OON]	[OOO]	[POO]	[OOO]	[OON]
Segment *2*	$\bar{U}_{S1p}$	$\bar{U}_{M1}$	$\bar{U}_{L1}$	$\bar{U}_{M1}$	$\bar{U}_{S1p}$
	[POO]	[PON]	[PNN]	[PON]	[POO]
Segment 3*a*	$\bar{U}_{S1p}$	$\bar{U}_{M1}$	$\bar{U}_{S2n}$	$\bar{U}_{M1}$	$\bar{U}_{S1p}$
	[POO]	[PON]	[OON]	[PON]	[POO]
Segment 3*b*	$\bar{U}_{S2n}$	$\bar{U}_{M1}$	$\bar{U}_{S1p}$	$\bar{U}_{M1}$	$\bar{U}_{S2n}$
	[OON]	[PON]	[POO]	[PON]	[OON]
Segment 4	$\bar{U}_{S2n}$	$\bar{U}_{M1}$	$\bar{U}_{L2}$	$\bar{U}_{M1}$	$\bar{U}_{S2n}$
	[OON]	[PON]	[PPN]	[PON]	[OON]

Power System Technology
ISSN:1000-3673
Received: 10-01-2024 Revised: 02-02-2024 Accepted: 04-03-2024

A distinctive feature of the 7-stage SS (see Table 2) is that to form the spatial voltage vector $\bar{U}_s$, only one small basic vector with a uniform distribution of *p*- and *n*-type states is used over one quantization period T_{PWM} in segments 2 and 4, and a uniform distribution of the combinations of *p*- and *n*-type states is ensured in segments 1 and 3 only for one small vector with a longer switching duration. Such a vector is called a dominant small basic vector. For example, if the spatial voltage vector $\bar{U}_s$ falls into segments 1*a* or 3*a* in the sector I (see Fig. 2), the vector $\bar{U}_{S1}$ is chosen as the dominant small basic vector, and the vector $\bar{U}_{S2}$ is used in segments 1*b* or 3*b*. The 7-stage SS ensures the lowest level of the NP voltage balance. This SS also contains the combinations of states from sector III (see Table 1) underlined in Table 2. As a result, these combinations of small basic vectors cause high CM voltage with the $\pm U_d/3$ level.

In a 7-stage SS, the spatial voltage vector $\bar{U}_s$ is formed due to three levels of switchings SL_1–SL_3 (Fig. 3a) when comparing them to the sawtooth voltage u_{SVG}, which requires six switchings of the basic vectors over one quantization period T_{PWM}. A transition between region *a* and *b* requires two additional switchings of basic vectors (see Table 2), and a transition from one segment (or sector) to another does not lead to additional switchings.

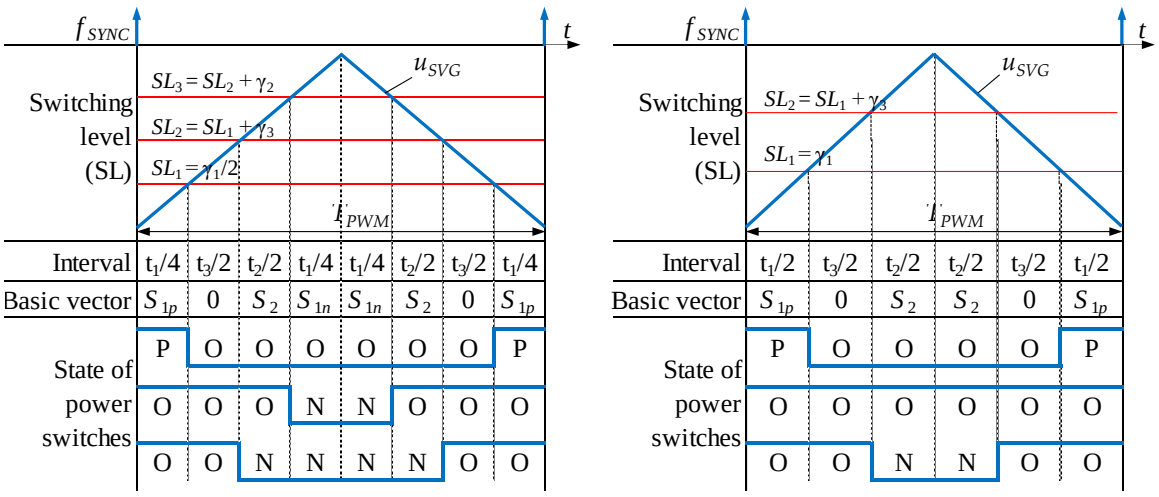

Fig. 3. The principle of switching basic vectors over one PWM period in segment 1*a* (sector I) for (a) the 7-stage and (b) 5-stage SS

The 5-stage SS (Table 3) is constructed by removing the combinations of sector III from Table 2, which provides a low CM voltage level compared to the 7-stage SS (see Table 1). The spatial voltage vector $\bar{U}_s$ is formed here due to two switching levels of SL_1 and SL_2 (see Fig. 3b), which requires only four switchings of basic vectors over one quantization period T_{PWM}. Similar to the 7-stage SS, in the 5-stage SS the transition between regions *a* and *b* also requires two

Power System Technology
ISSN:1000-3673
Received: 10-01-2024 Revised: 02-02-2024 Accepted: 04-03-2024

additional switchings of basic vectors (see Table 3), and the transition from one segment (or sector) to another does not lead to additional switchings. We can conclude that switching losses in a 5-stage SS will be minimal compared to a 7-stage SS. In a 5-stage SS, only one of two types (P or N) of combinations of small basic vectors is used in each segment over one switching period T_{PWM}, which leads to the NP voltage imbalance. This is the main drawback of this SS. In practice, the use of a 5-stage SS overestimates the parameters of power equipment, for example, the capacitances of DC link capacitors, increases the weight–size parameters of high-frequency filters at the inverter output, etc.

Thus, the separate use of the 5-stage and 7-stage SS leads to significant drawbacks in the control of three-level inverters. This paper proposes an algorithm of a SVPWM with a hybrid SS to minimize the drawbacks outlined above.

3. Synthesis of a hybrid switching sequence for the SVPWM algorithm

Expression (1) indicates that the degree of influence of the nearest basic vector in any of the segments on a given spatial vector depends on the relative switching duration γ_i, the increase of which augments the influence on the spatial vector. As a result, the spatial vector has many of the properties of the basic vector itself. Figures 4a and 4b show the degree of influence of the three closest basic vectors on the position of the spatial vector using the example of 1 segment (sector I).

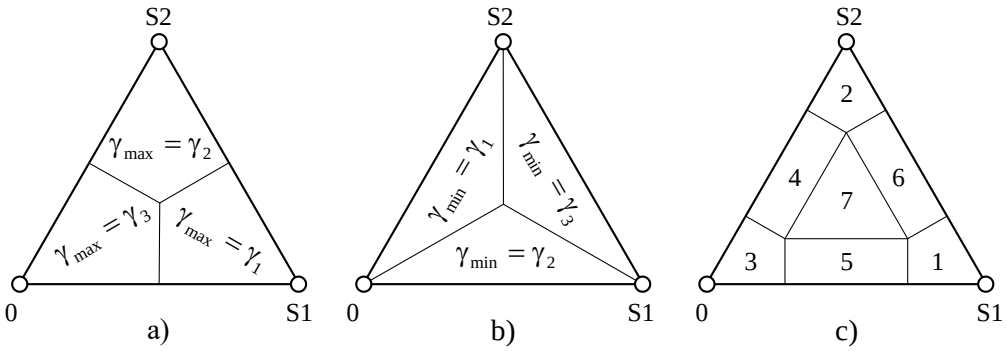

Fig. 4. The relationship between the position of the spatial vector and the duration of switching the basic vectors using the example of 1 segment (sector I)

Here the maximum and minimum relative durations are determined as:

$$\begin{cases}\gamma_{max}=\max(\gamma_1,\gamma_2,\gamma_3);\\ \gamma_{min}=\min(\gamma_1,\gamma_2,\gamma_3).\end{cases} \quad (2)$$

However, the influence of the three closest basic vectors on a given spatial voltage vector does not differ significantly in the central segment region. Therefore, we proposed dividing any

Power System Technology
ISSN:1000-3673
Received: 10-01-2024 Revised: 02-02-2024 Accepted: 04-03-2024

segment into seven regions (see Fig. 4c). Then we can see that the basic vector $\bar{U}_{S1}$ provides the strongest influence on a given spatial vector in region 1 and the weakest influence in region 4; the basic vector $\bar{U}_{S2}$ provides the strongest influence in region 2 and the weakest influence in region 5; the basic vector $\bar{U}_0$ provides the strongest influence in region 3 and the weakest influence in region 6; and the influence of the three basic vectors in region 7 is not significantly different.

Let us consider a hybrid SS in such a way as to ensure a low level of the NP and CM voltage in the system. As is known, when modulating the spatial voltage vector, two small basic vectors are used in segments 1 and 3, and only one small vector is used in segments 2 and 4 (Fig. 1).

3.1. Synthesis of a hybrid switching sequence for segment 1 and 3

According to (1), the spatial voltage vector $\bar{U}_s$ in segment 1 can be described by the combinations of the states of small basic vectors $\bar{U}_{S1}$([POO],[ONN]) and $\bar{U}_{S2}$ ([OON],[PPO]), as well as one zero vector $\bar{U}_0$([PPP],[OOO],[NNN]):

$$\begin{cases} \bar{U}_s = \gamma_1 \begin{Bmatrix} [\mathrm{POO}] \\ [\mathrm{ONN}] \end{Bmatrix} + \gamma_2 \begin{Bmatrix} [\mathrm{PPO}] \\ [\mathrm{OON}] \end{Bmatrix} + \gamma_3 \begin{Bmatrix} [\cancel{\mathrm{PPP}}] \\ [\mathrm{OOO}] \\ [\cancel{\mathrm{NNN}}] \end{Bmatrix}; \\ \gamma_1 + \gamma_2 + \gamma_3 = 1. \end{cases} \tag{3}$$

Here, the combinations of the [PPP] and [NNN] states of the zero basic vector are immediately excluded since they cause the maximum CM voltage $\pm U_d/2$ (see Table 1). Notably:

- $\bar{U}_0$[OOO] does not affect the NP voltage and ensures zero CM voltage (see Table 1);

- $\bar{U}_{S1}$([POO],[ONN]), $\bar{U}_{S2}$([OON],[PPO]) significantly affect the NP voltage. $\bar{U}_{S1p}$, $\bar{U}_{S2n}$ provide a low CM voltage, and $\bar{U}_{S1n}$, $\bar{U}_{S2p}$ cause a high CM voltage $\pm U_d/3$. Consequently, the two $\bar{U}_{S1n}$, $\bar{U}_{S2p}$ combinations are used only in the 7-stage SS (see Table 2) to ensure NP voltage balance.

The 5-stage SS has *p*-type combinations $\bar{U}_{S1p}$ and *n*-type combinations $\bar{U}_{S2n}$ (see Table 3), which ensures NP voltage balance only when the duration of their switchings is approximately equal to each other or when the end of the spatial voltage vector $\bar{U}_s$ is located near the boundary between segments 1*a* and 1*b*. As the end of the vector $\bar{U}_s$ approaches the end of the zero basic vector $\bar{U}_0$, its influence on the vector $\bar{U}_s$ increases, while the influence of the vectors $\bar{U}_{S1}$ and

Power System Technology
ISSN:1000-3673
Received: 10-01-2024 Revised: 02-02-2024 Accepted: 04-03-2024

$\bar{U}_{S2}$ decreases. Therefore, the application area of the 5-stage SS between segments 1*a* and 1*b* can be expanded when approaching the end of the zero basic vector $\bar{U}_0$. The remaining regions are meant for the seven-stage SS.

Based on the above analysis, segment 1 can be divided into four regions, as shown in Fig. 5a. Here, the switching of the 7-stage SS corresponds to regions s_1 and s_2, and the switching of the 5-stage SS corresponds to regions f_1 and f_2.

Similarly, segment 3 is also divided into four regions, as shown in Fig. 5b. Here, the switching of the 7-stage SS corresponds to regions s_1 and s_2, and the switching of the 5-stage SS corresponds to regions f_1 and f_2.

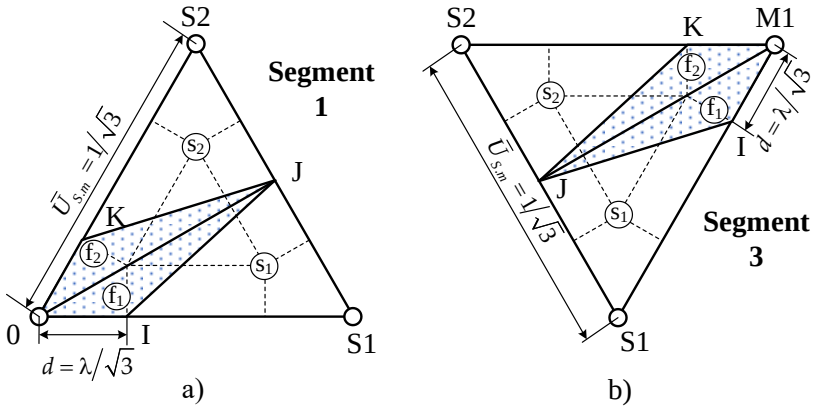

Fig. 5. Hybrid SS for (a) the 1st and (b) 3rd segments in sector I

3.2. Synthesis of a hybrid switching sequence for segments 2 and 4

The spatial voltage vector $\bar{U}_s$ in segment 2 (see Fig. 2) can be described by the combinations of the states of the large basic $\bar{U}_{L1}$[PNN], medium $\bar{U}_{M1}$[PON], and small vector $\bar{U}_{S1}$ ([POO],[ONN]):

$$\begin{cases} \bar{U}_s = \gamma_1[\text{PNN}] + \gamma_2[\text{PON}] + \gamma_3 \begin{Bmatrix} [\text{POO}] \\ [\text{ONN}] \end{Bmatrix}; \\ \gamma_1 + \gamma_2 + \gamma_3 = 1. \end{cases} \tag{4}$$

Notably:

- $\bar{U}_{M1}$[PON] insignificantly affects the NP voltage and ensures a zero CM voltage (see Table 1);

- $\bar{U}_{L1}$[PNN] does not affect the NP voltage and ensures a low CM voltage;

Power System Technology
ISSN:1000-3673
Received: 10-01-2024 Revised: 02-02-2024 Accepted: 04-03-2024

- $\bar{U}_{S1}$([POO],[ONN]) significantly affects the NP voltage. $\bar{U}_{S1p}$ ensures a low CM voltage, while $\bar{U}_{S1n}$ causes a high CM voltage $\pm U_d$ /3 (see Table 1). Consequently, the $\bar{U}_{S1n}$ combination is used only in the 7-stage SS (Table 2) to ensure the NP voltage balance jointly with $\bar{U}_{S1p}$.

The 5-stage SS has only one combination type of the state of the small basic vector $\bar{U}_{S1p}$, which leads to NP voltage imbalance. Therefore, we should select regions for the switching of the 5-stage SS where the small basic vector has a weak influence on vector $\bar{U}_s$, while the medium or large basic vectors have a strong influence. This means that as the end of vector $\bar{U}_s$ approaches vector $\bar{U}_{S1}$, the use of the 7-stage SS should increase, while the use of the 5-stage SS should sharply decrease.

Based on this analysis, segment 2 can be divided into two regions, as shown in Fig. 6a. Here, the switching of the 7-stage SS corresponds to region s, and the switching of the 5-stage SS corresponds to region f.

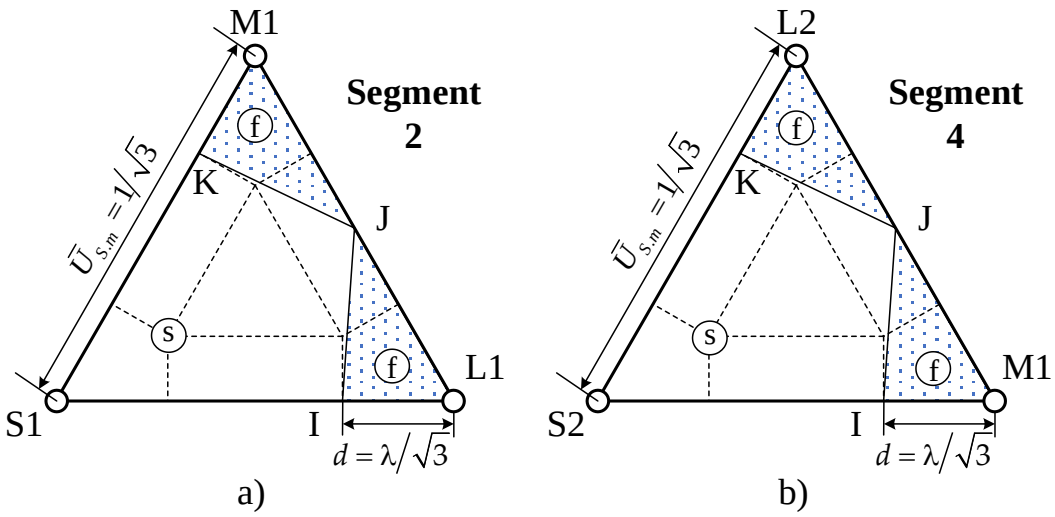

Fig. 6. Hybrid SS for the (a) 2nd and (b) 4th segments in sector I

Similarly, segment 4 is also divided into two regions as shown in Fig. 6b. The 7-stage SS is switched in region s, and the 5-stage SS is switched in region f.

Based on Tables 2 and 3, as well as Fig. 5 and 6, we synthesized a hybrid SS. Table 4 shows that the transition between a 5-stage and 7-stage SS does not require additional switching pairs for basic vectors.

Power System Technology
ISSN:1000-3673
Received: 10-01-2024 Revised: 02-02-2024 Accepted: 04-03-2024

3.3. Conditions for switching between the regions in a hybrid switching sequence

To improve the four main indicators in the system (the quality of the inverter output current, the NP voltage, the CM voltage, and the switching losses of power switches), the hybrid SS provides for switching between regions corresponding to the switching of the 5-stage and 7-stage SS when the system operates in each segment, i.e., we shall determine the operating regions of these SS on the complex plane (vector diagram). With this in mind, let us introduce the regulation coefficient λ of the hybrid SS, which is determined as:

$$\lambda = \frac{d}{\bar{U}_{S.m}} = d\sqrt{3} \quad \text{when} \quad 0 \le \lambda \le 1, \tag{5}$$

where $\bar{U}_{S.m} = 1/\sqrt{3}$ is the normalized value of the small basic vector modulus equal to the length of the segment side; *d* is a part of the length of the segment side corresponding to the switching of a 5-stage SS (regions f_1 and f_2) according to Fig. 5 for the 1st and 3rd segments, and region f for the 2nd and 4th segments (see Fig. 6).

Based on Fig. 5 and 6, we determined the conditions for switching between the regions in the hybrid SS for each segment, which are summarized in Table 5.

Table 4. A hybrid SS for sector I

Segment 1								***Segment 2***			
f_1		**f_2**		**s_1**		**s_2**		**f**		**s**	
$\bar{U}_{S1p}$	[POO]	$\bar{U}_{S2n}$	[OON]	$\bar{U}_{S1p}$	[POO]	$\bar{U}_{S2n}$	[OON]	$\bar{U}_{S1p}$	[POO]	$\bar{U}_{S1p}$	[POO]
$\bar{U}_0$	[OOO]	$\bar{U}_0$	[OOO]	$\bar{U}_0$	[OOO]	$\bar{U}_0$	[OOO]	$\bar{U}_{M1}$	[PON]	$\bar{U}_{M1}$	[PON]
$\bar{U}_{S2n}$	[OON]	$\bar{U}_{S1p}$	[POO]	$\bar{U}_{S2n}$	[OON]	$\bar{U}_{S1p}$	[POO]	$\bar{U}_{L1}$	[PNN]	$\bar{U}_{L1}$	[PNN]
$\bar{U}_0$	[OOO]	$\bar{U}_0$	[OOO]	$\bar{U}_{S1n}$	[ONN]	$\bar{U}_{S2p}$	[PPO]	$\bar{U}_{M1}$	[PON]	$\bar{U}_{S1n}$	[ONN]
$\bar{U}_{S1p}$	[POO]	$\bar{U}_{S2n}$	[OON]	$\bar{U}_{S2n}$	[OON]	$\bar{U}_{S1p}$	[POO]	$\bar{U}_{S1p}$	[POO]	$\bar{U}_{L1}$	[PNN]
				$\bar{U}_0$	[OOO]	$\bar{U}_0$	[OOO]			$\bar{U}_{M1}$	[PON]
				$\bar{U}_{S1p}$	[POO]	$\bar{U}_{S2n}$	[OON]			$\bar{U}_{S1p}$	[POO]
Segment 3								***Segment 4***			
f_1		**f_2**		**s_1**		**s_2**		**f**		**s**	
$\bar{U}_{S1p}$	[POO]	$\bar{U}_{S2n}$	[OON]	$\bar{U}_{S1p}$	[POO]	$\bar{U}_{S2n}$	[OON]	$\bar{U}_{S2n}$	[OON]	$\bar{U}_{S2n}$	[OON]

Power System Technology
ISSN:1000-3673
Received: 10-01-2024 Revised: 02-02-2024 Accepted: 04-03-2024

$\bar{U}_{M1}$	[PON]	$\bar{U}_{M1}$	[PON]	$\bar{U}_{M1}$	[PON]	$\bar{U}_{M1}$	[PON]	$\bar{U}_{M1}$	[PON]	$\bar{U}_{M1}$	[PON]
$\bar{U}_{S2n}$	[OON]	$\bar{U}_{S1p}$	[POO]	$\bar{U}_{S2n}$	[OON]	$\bar{U}_{S1p}$	[POO]	$\bar{U}_{L2}$	[PPN]	$\bar{U}_{L2}$	[PPN]
$\bar{U}_{M1}$	[PON]	$\bar{U}_{M1}$	[PON]	$\bar{U}_{S1n}$	[ONN]	$\bar{U}_{S2p}$	[PPO]	$\bar{U}_{M1}$	[PON]	$\bar{U}_{S2p}$	[PPO]
$\bar{U}_{S1p}$	[POO]	$\bar{U}_{S2n}$	[OON]	$\bar{U}_{S2n}$	[OON]	$\bar{U}_{S1p}$	[POO]	$\bar{U}_{S2n}$	[OON]	$\bar{U}_{L2}$	[PPN]
				$\bar{U}_{M1}$	[PON]	$\bar{U}_{M1}$	[PON]			$\bar{U}_{M1}$	[PON]
				$\bar{U}_{S1p}$	[POO]	$\bar{U}_{S2n}$	[OON]			$\bar{U}_{S2n}$	[OON]

The conditions for switching between the two types of SSs (see Table 5) show that their operating region depends on the regulation coefficient λ of the hybrid SS and the relative durations γ_1 and γ_2 associated with the position of the spatial voltage vector $\bar{U}_s(\mu, \theta)$ (see Fig. 2). Here μ is the modulation coefficient, which sets the length of the vector $\bar{U}_s$, and θ it its angle of rotation.

Table 5. Conditions for switching between the regions in the hybrid SS

Segments 1 and 3			
Region s_1	Region s_2	Region f_1	Region f_2
$\begin{cases}\gamma_1 \geq \gamma_2 \\ \gamma_1 + (2\lambda - 1)\gamma_2 \geq \lambda\end{cases}$	$\begin{cases}\gamma_1 < \gamma_2 \\ (2\lambda - 1)\gamma_1 + \gamma_2 \geq \lambda\end{cases}$	$\begin{cases}\gamma_1 \geq \gamma_2 \\ \gamma_1 + (2\lambda - 1)\gamma_2 < \lambda\end{cases}$	$\begin{cases}\gamma_1 < \gamma_2 \\ (2\lambda - 1)\gamma_1 + \gamma_2 < \lambda\end{cases}$
Segments 2 and 4			
Region s		Region f	
$\begin{cases}\gamma_1 + (1 - 2\lambda)\gamma_2 \leq 1 - \lambda \\ (1 - 2\lambda)\gamma_1 + \gamma_2 \leq 1 - \lambda\end{cases}$		$\begin{cases}\gamma_1 + (1 - 2\lambda)\gamma_2 > 1 - \lambda \\ (1 - 2\lambda)\gamma_1 + \gamma_2 > 1 - \lambda\end{cases}$	

Figure 7 shows the dependence of the operating range of the 5-stage and 7-stage SS on the coefficients μ and λ, which allows us to draw the following conclusions:

- at $\lambda = 0$ only a 7-stage SS is used, while at $\lambda = 1$ only a 5-stage SS is used (see Table 5);

Power System Technology
ISSN:1000-3673
Received: 10-01-2024 Revised: 02-02-2024 Accepted: 04-03-2024

- at $0 < d = d_1 \le \sqrt{3}/4$ (i.e. $0 < \lambda \le 0.75$) and $0 \le \mu \le r_1 = d$ or at $\sqrt{3}/4 < d = d_2 < 1/\sqrt{3}$ (i.e. $0.75 < \lambda < 1$) and $\mu \le r_2$, only the 5-stage SS is switched (see Fig. 7b). Here r_2 is the radius of the circle tangent to the straight line Td_2;

- with an increase in the regulation coefficient λ, the overall operating range of the 5-stage SS expands, while that of the 7-stage SS narrows, and vice versa (see Fig. 7 b);

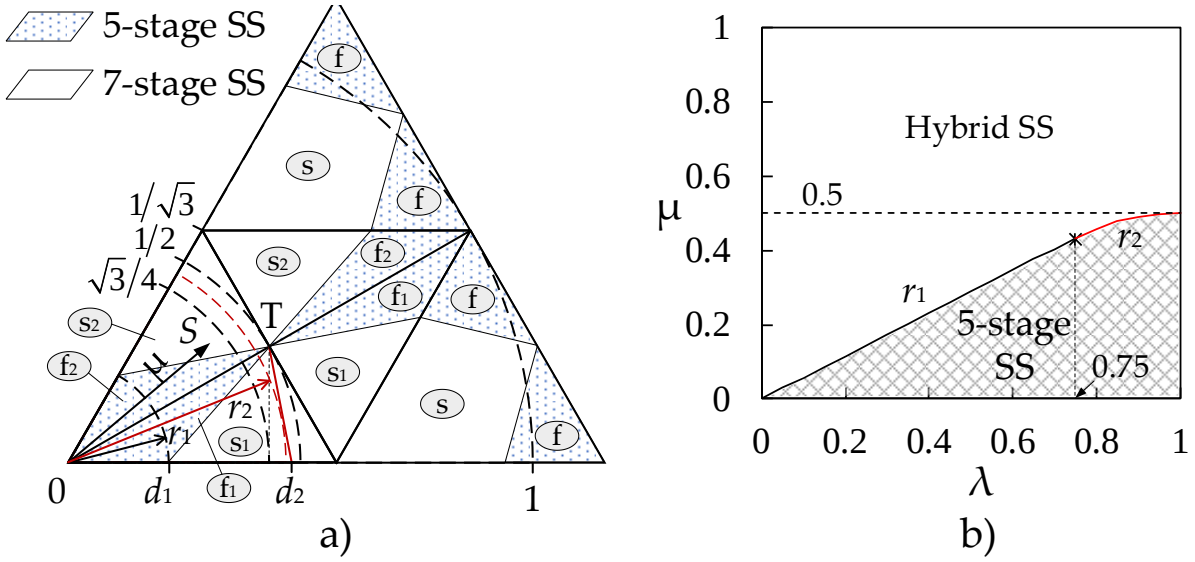

Fig. 7. Vector diagram of a hybrid SS for (a) one sector and (b) the dependence of the operating range of the SS type on the coefficients μ and λ

- with an increase in the modulation coefficient μ in the range from r_1 to 0.5 (or from r_2 to 0.5) the overall operating range of the 7-stage SS widens, while that of the 5-stage SS narrows;

- with an increase in the coefficient μ in the range from 0.5 to 1, the overall operating range of the 7-stage SS narrows, while that of the 5-stage SS widens.

4. A system to control a SVPWM with a hybrid switching sequence

Figure 8 shows the functional diagram of the control system of a 3L NPC VSI implementing the algorithm for a SVPWM with a hybrid SS. It consists of the following main units: sawtooth voltage and synchronized pulse generator (SVG); SVPWM calculator, which includes a sector and segment number determinant and a sector face projection calculator, and γ_1, γ_2, γ_3 coefficient calculator; and a hybrid SS unit. The operation of these units, with the exception of the hybrid SS unit, is discussed in detail in [28].

The sawtooth voltage and synchronized pulse generator generate the sawtooth voltage u_{SVG} with a frequency of T_{PWM} and synchronizing pulses f_{SYNC} when the signal u_{SVG} passes through the zero level (see Fig. 3).

Power System Technology
ISSN:1000-3673
Received: 10-01-2024 Revised: 02-02-2024 Accepted: 04-03-2024

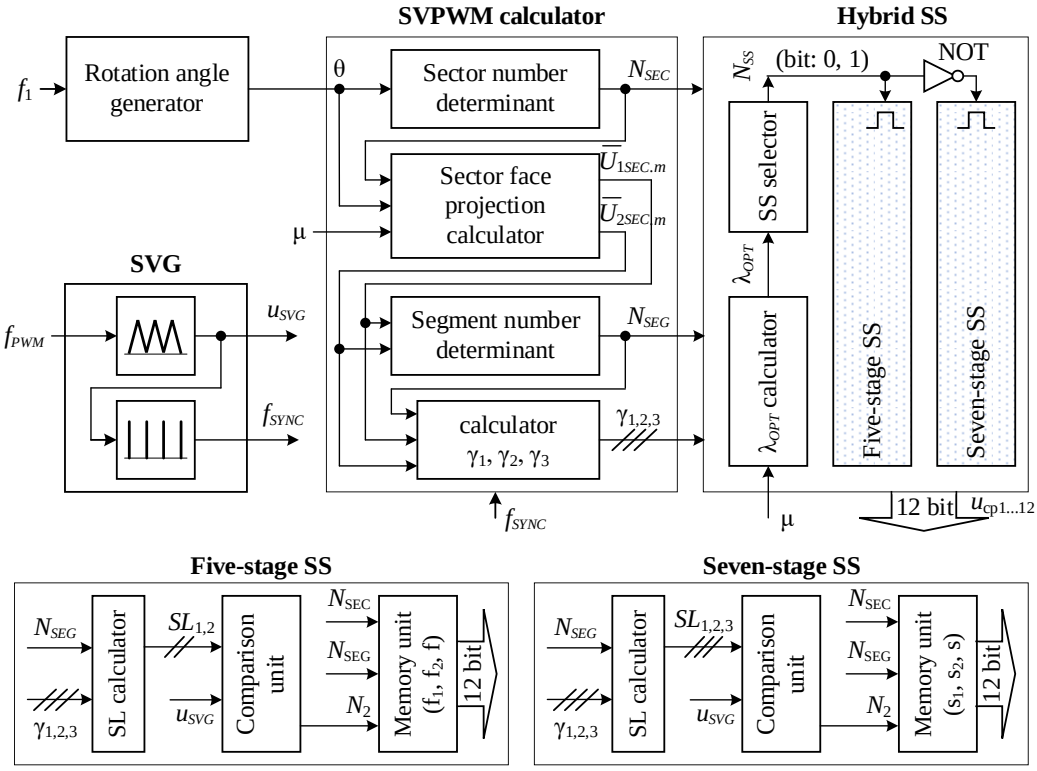

Fig. 8. Functional diagram of the control system of the algorithm for a SVPWM with a hybrid SS for a 3L NPC VSI

The rotation angle generator generates the rotation angle θ of the spatial voltage vector in the system (see Fig. 2) depending on the inverter command signal at the frequency f_1 according to:

$$\begin{cases} \theta = \int_0^{2\pi} 2\pi f_1 \cdot dt, \text{ if } \theta < 2\pi; \\ \theta = 0, \text{ if } \theta = 2\pi. \end{cases} \tag{6}$$

The SVPWM calculator calculates the relative switching durations of the basic vectors γ_1, γ_2 and γ_3, and determines the numbers of the sector N_{SEC} and the segment N_{SEG} with the spatial voltage sector $\bar{U}_s$ (see Fig. 2) in real time. Since the system is digital, all changes at the unit outputs occur under the influence of synchronizing pulses f_{SYNC} (see Fig. 3).

The "Sector number determinant" unit generates an integer $N_{SEC} = 1 \ldots 6$ at the output depending on the position of the spatial vector $\bar{U}_s$ in the vector diagram (see Fig. 2) according to:

Power System Technology
ISSN:1000-3673
Received: 10-01-2024 Revised: 02-02-2024 Accepted: 04-03-2024

$$\begin{cases} N_{SEC}=1, \text{if } 0\le\theta<\pi/3; \\ N_{SEC}=2, \text{if } \pi/3\le\theta<2\pi/3; \\ N_{SEC}=3, \text{if } 2\pi/3\le\theta<\pi; \\ N_{SEC}=4, \text{if } \pi\le\theta<4\pi/3; \\ N_{SEC}=5, \text{if } 4\pi/3\le\theta<5\pi/3; \\ N_{SEC}=6, \text{if } 5\pi/3\le\theta<2\pi. \end{cases} \tag{7}$$

The "Segment number determinant" unit generates an integer N_{SEG} = 1…4 at the output also depending on the position of the spatial vector $\bar{U}_s$ in the vector diagram (see Fig. 2). Table 6 summarizes the spatial vector membership conditions for all four segments.

To determine the number of the segment N_{SEG}, we use the projections of the spatial voltage vector $\bar{U}_s$ onto the corresponding faces of the sector $U_{1SEC.m}$ and $U_{2SEC.m}$ (see Fig. 2) written in relative units with respect to the maximum amplitude of the spatial vector $U_{m.\max}=U_d/\sqrt{3}$:

$$\begin{cases} \bar{U}_{1SEC.m}=\dfrac{U_{1SEC.m}}{U_{m.\max}}=\dfrac{2}{\sqrt{3}}\cdot\mu\,\sin\left[N_{SEC}\cdot\pi/3-\theta\right]; \\ \bar{U}_{2SEC.m}=\dfrac{U_{2SEC.m}}{U_{m.\max}}=\dfrac{2}{\sqrt{3}}\cdot\mu\,\sin\left[\theta-(N_{SEC}-1)\cdot\pi/3\right], \end{cases} \tag{8}$$

where $\mu=U_m/U_{m.\max}$ is the modulation coefficient specifying the length of the spatial vector $\bar{U}_s$. The system of equations (8) is solved in the "Sector face projection calculator" unit (see Fig. 8).

The relative switching durations of the basic vectors γ_1, γ_2 and γ_3 over each PWM period are calculated according to the equations given in Table 6 for any segment. Here, the coefficients γ_1, γ_2, γ_3 are calculated based on the projections of the spatial voltage vector $\bar{U}_s$ onto the corresponding faces of the sector $U_{1SEC.m}$ and $U_{2SEC.m}$ (see Fig. 2).

Table 6. Mathematical expressions to determine the segment number and calculate the relative durations of basic vector activations in relative units

Segment number	Membership conditions	Relative durations of basic vector activations
1	$\begin{cases}\bar{U}_{1SEC.m}\le 1/\sqrt{3}; \\ \bar{U}_{2SEC.m}\le 1/\sqrt{3}; \\ \bar{U}_{1SEC.m}+\bar{U}_{2SEC.m}\le 1/\sqrt{3}.\end{cases}$	$\begin{cases}\gamma_1=\bar{U}_{1SEC.m}/\bar{U}_{S.m}=\sqrt{3}\cdot\bar{U}_{1SEC.m}; \\ \gamma_2=\bar{U}_{2SEC.m}/\bar{U}_{S.m}=\sqrt{3}\cdot\bar{U}_{2SEC.m}; \\ \gamma_3=1-(\gamma_1+\gamma_2).\end{cases}$

Power System Technology
ISSN:1000-3673
Received: 10-01-2024 Revised: 02-02-2024 Accepted: 04-03-2024

2	$\bar{U}_{1SEC.m} > 1/\sqrt{3}$.	$\begin{cases}\gamma_1 = \left(\bar{U}_{1SEC.m}/\bar{U}_{S.m}\right) - 1 = \sqrt{3}\cdot\bar{U}_{1SEC.m} - 1;\\ \gamma_2 = \bar{U}_{2SEC.m}/\bar{U}_{S.m} = \sqrt{3}\cdot\bar{U}_{2SEC.m};\\ \gamma_3 = 1-(\gamma_1+\gamma_2).\end{cases}$
3	$\begin{cases}\bar{U}_{1SEC.m} \le 1/\sqrt{3};\\ \bar{U}_{2SEC.m} \le 1/\sqrt{3};\\ \bar{U}_{1SEC.m} + \bar{U}_{2SEC.m} > 1/\sqrt{3}.\end{cases}$	$\begin{cases}\gamma_1 = 1-\left(\bar{U}_{2SEC.m}/\bar{U}_{S.m}\right) = 1-\sqrt{3}\cdot\bar{U}_{2SEC.m};\\ \gamma_2 = 1-\left(\bar{U}_{1SEC.m}/\bar{U}_{S.m}\right) = 1-\sqrt{3}\cdot\bar{U}_{1SEC.m};\\ \gamma_3 = 1-(\gamma_1+\gamma_2).\end{cases}$
4	$\bar{U}_{2SEC.m} > 1/\sqrt{3}$.	$\begin{cases}\gamma_1 = \bar{U}_{1SEC.m}/\bar{U}_{S.m} = \sqrt{3}\cdot\bar{U}_{1SEC.m};\\ \gamma_2 = \left(\bar{U}_{2SEC.m}/\bar{U}_{S.m}\right) - 1 = \sqrt{3}\cdot\bar{U}_{2SEC.m} - 1;\\ \gamma_3 = 1-(\gamma_1+\gamma_2).\end{cases}$

The hybrid SS unit generates control pulses u_{cp1}...u_{cp12} to control the inverter power switches and consists of the following units: optimal regulation coefficient λ_{OPT} calculator, SS selector, and 5-stage and 7-stage SS units (see Fig. 8).

The λ_{OPT} calculator calculates the optimal regulation coefficient depending on the modulation coefficient μ. The mathematics of this unit will be discussed in detail in section 5.3.

The SS selector switches between the 5-stage or 7-stage SS depending on the position of the spatial voltage vector $\bar{U}_s$ according to the conditions given in Table 5. Here the regulation coefficient λ should be replaced by the optimal coefficient λ_{OPT}. The output of this unit N_{SS} is a logical signal: 0 for the 7-stage SS and 1 for the 5-stage SS.

The 5-stage SS and 7-stage SS units generate control signals to activate the inverter power switches according to the 7-stage (Table 2) and 5-stage (Table 3) SS operating algorithm and consist of the following subunits: SL calculator, comparison unit, and memory units (Fig. 8).

The SL calculator calculates two switching levels for the 5-stage SS according to $SL_1 = \gamma_i$ and $SL_2 = SL_1 + \gamma_j$ (see Fig. 3b), where *i, j* are integers from 1 to 3, which depend on the position of the spatial vector $\bar{U}_s$ in each segment. Three switching levels are calculated for the 7-stage SS so that the total switching duration of *p*-type combinations of small basic vectors is equal to the switching duration of *n*-type combinations based on $SL_1 = \gamma_i/2$, $SL_2 = SL_1 + \gamma_j$, $SL_3 = SL_2 + \gamma_k$ (see Fig. 3a), where i, j, k are integers from 1 to 3.

Comparison units consist of two comparators in the 5-stage SS and three comparators in the 7-stage SS, which compare the sawtooth voltage u_{SVG} with the switching levels SL_n for each

Power System Technology
ISSN:1000-3673
Received: 10-01-2024 Revised: 02-02-2024 Accepted: 04-03-2024

PWM period (see Fig. 3) to determine the switching time of the basic vectors that form the spatial vector voltage on the vector diagram plane (see Fig. 2), where *n* is an integer from 1 to 3. The output data are encoded with the two-bit binary code N_2 containing information on the address of the memory cell with the information on the activation of a particular basic vector.

The memory unit stores information on the power switch activation status codes for the 5-stage and 7-stage SS according to Table 4. Memory cells are accessed depending on the sector N_{SEC}, the segment N_{SEG}, and the binary code N_2 from the output of the comparison unit.

5. Simulation of a three-level neutral point clamped voltage source inverter with a SVPWM and a hybrid switching sequence

We designed a computer model in the *MatLab+Simulink* environment to assess the effectiveness of the proposed inverter control algorithm (see Fig. 8) in terms of the quality of the current curve at the inverter output, NP voltage, switching losses, and CM voltage. The model used a 500V DC voltage source with low internal resistance to power the inverter. All the studies were carried out under an active-inductive load with an active resistance of 100 Ohms and cosφ = 0.8. The PWM frequency of the spatial voltage vector was taken to be 5 kHz and the basic frequency at the inverter output was f_1 = 50Hz.

5.1 Quantitative indicators of the simulation results

The quality of the current curve at the inverter output was assessed by the distortion coefficient of higher current harmonics:

$$\mathrm{THD}i = \frac{\sqrt{\sum_{n=2}^{\infty} I_{m(n)}^2}}{I_{m(1)}}, \tag{9}$$

where $I_{m(n)}$ is the amplitude of the higher current harmonics at the output of the VSI in relation to the first current harmonic $I_{m(1)}$.

The NP voltage balance provides the condition $u_{NP} = U_d/2$, otherwise there is a deviation in the NP voltage $\Delta u_{NP} = u_{NP} - U_d/2$. The effectiveness of the NP voltage balance was assessed based on the maximum value of the relative NP voltage error:

$$\delta u_{NP.m} = \frac{|\Delta u_{NP}|_{\max}}{U_d/2} \cdot 100\%. \tag{10}$$

The level of switching losses was assessed by the number of switching pairs of power switches N_{SW} over one period of the fundamental voltage harmonic at the inverter output. To assess the effectiveness of the algorithm, we used the indicator of the relative reduction in the number of

Power System Technology
ISSN:1000-3673
Received: 10-01-2024 Revised: 02-02-2024 Accepted: 04-03-2024

switching pairs of power switches n_{SW} in relation to the 7-stage SS ($\lambda = 0$), since at a given SS, the maximum number of switchings observed in the system is:

$$n_{SW} = \frac{N_{SW}}{N_{SW(\lambda=0)}} \cdot 100\% . \tag{11}$$

As noted, when the 7-stage SS is used, high CM voltage equal to $\pm U_d/3$ appears in the output voltage of the VSI (see Tables 1 & 2). Therefore, to assess the CM voltage, we use the pulse duty factor γ_{CM} with the $\pm U_d/3$ level over one period of the fundamental voltage harmonic at the inverter output:

$$\gamma_{CM} = \frac{\sum_{i=1}^{n} t_{CM.i}}{T_1} \cdot 100\% , \tag{12}$$

where $t_{CM.i}$ is the time interval of the i-th appearance of the high CM voltage with the $\pm U_d/3$ level over one period T_1 of the inverter output voltage (see Fig. 9).

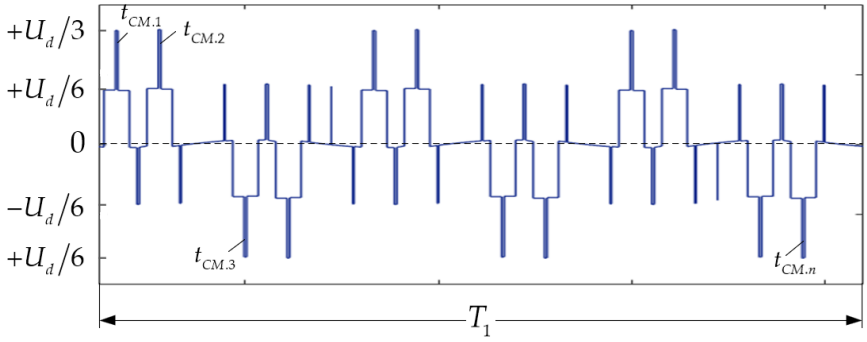

Fig. 9. CM voltage time diagrams over one period of the fundamental voltage harmonic at the output of a 3L VSI

5.2 Analysis of the simulation results

Based on the computer model of a 3L VSI and the algorithm for a SVPWM with a hybrid SS (see Fig. 8), Fig. 10 shows the static state spaces: the distortion coefficient of the higher current harmonics THDi at the inverter output, the maximum relative NP voltage error $\delta u_{NP.m}$, the relative reduction in the number of switching pairs of power switches n_{SW}, and the CM voltage pulses duty factor γ_{CM} with the $\pm U_d/3$ level over one period of the fundamental voltage harmonic at the inverter output, depending on the modulation coefficient μ and the regulation coefficient λ of the hybrid SS.

Power System Technology
ISSN:1000-3673

Received: 10-01-2024 Revised: 02-02-2024 Accepted: 04-03-2024

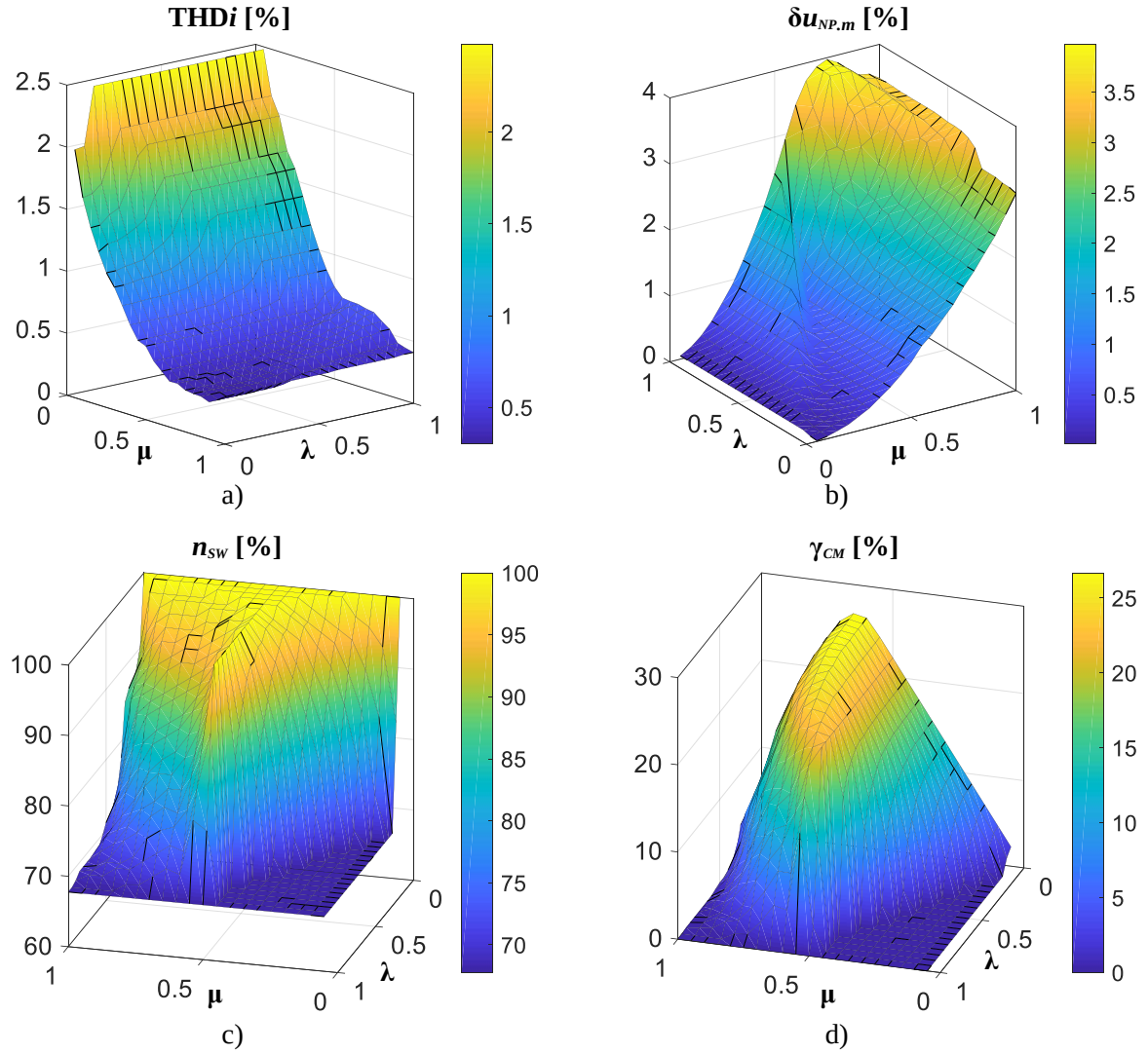

Fig. 10. Static state spaces: (a) the distortion coefficient of higher current harmonics THD*i* at the VSI output; (b) the maximum relative NP voltage error $\delta u_{NP.m}$; (c) the relative reduction in the number of switching pairs of power switches n_{SW}; and (d) the CM voltage pulse duty factor γ_{CM} when changing the coefficients μ and λ

The analysis of the static state spaces allows drawing the following conclusions:

– The distortion coefficient of higher current harmonics THD*i* at the VSI output reaches 2.5% at a modulation coefficient μ close to zero for the SVPWM with a 5-stage SS ($\lambda = 1$) and 2.0% for a 7-stage SS ($\lambda = 0$) (see Fig 10a). This is explained by the fact that three switching levels are used to form the spatial voltage vector with a 7-stage SS (see Fig. 3a), and only two levels are used to form a 5-stage SS (see Fig. 3b). As a result, the accuracy of generating the VSI output voltage and, therefore, the current increases in the 7-stage SS. The SVPWM with a

Power System Technology
ISSN:1000-3673
Received: 10-01-2024 Revised: 02-02-2024 Accepted: 04-03-2024

hybrid SS occupies an average position between the 7-stage and 5-stage SS by the THD*i* level, which depends on the regulation coefficient λ. As the modulation coefficient μ decreases, the THD*i* coefficient increases for any λ values, since the amplitude of the first current harmonic at the inverter output decreases under an active-inductive load and the influence of higher current harmonics is more pronounced, as can be seen from expression (9).

– The relative NP error in the DC link of the VSI increases monotonically for a 7-stage SS ($\lambda = 0$) with an increase in the modulation coefficient μ and reaches its maximum value $\delta u_{NP.m} = 3.0\%$ at $\mu = 1.0$ (see Fig. 10b). This error is explained by the fact that in order to form the spatial voltage vector in the 7-stage SS in the range $0 < \mu \le 0.5$, we use small dominant basic vectors, which do not fully compensate for the time between the basic vectors of *p*- and *n*-types over one switching period. At $\mu > 0.5$, the error $\delta u_{NP.m}$ is explained by both the switching of small dominant vectors in the 3rd segment and the use of the average basic vectors in segments 2, 3, and 4 (see Fig. 2). For a 5-stage SS ($\lambda = 1$), the maximum relative error $\delta u_{NP.m}$ reaches 4.0 % at $\mu = 0.75$ but not at $\mu = 1$ and is 3.5% (Fig. 10b) because of the strong influence of the combinations of *p*- or *n*-type states of the small basic vectors at $\mu = 0.75$. As the coefficient increases $\mu > 0.75$, their switching duration decreases due to an increase in the switching time of the medium basic vectors. The SVPWM with a hybrid SS occupies an average position between the 7-stage and 5-stage SS by the error level $\delta u_{NP.m}$, which depends on the regulation coefficient λ. There are values of the coefficient λ when the NP voltage balance in the hybrid SS is close to the 7-stage SS by error level, which is achieved by switching the 7-stage SS compensating for the increase in the deviation of the NP error due to the operation of the 5-stage SS. So, for example, at $\mu = 0.35$ the maximum value of $\delta u_{NP.m} = 1.26\%$ when only the 5-stage SS is used, 0.42% when only the 7-stage SS is used, and 0.45% when a hybrid SS is used with $\mu = 0.4$.

– The relative number of switching pairs of power switches n_{SW} reaches 100% for the 7-stage SS ($\lambda = 0$) and decreases to 68% for the 5-stage SS ($\lambda = 1$) (see Fig. 10c) because the 7-stage SS has six switchings of basic vectors over one switching period, while the 5-stage SS has only four (see Fig. 3). For the SVPWM with a hybrid SS, the relative number of switchings of power switches n_{SW} depends on the regulation coefficient λ and varies from 68% to 100%. When the modulation coefficient μ is in the region of 0.5, the number of switching pairs of power switches n_{SW} reaches its maximum for the hybrid SS, which is explained by a significant expansion of the operating range of the 7-stage SS, while the operating range of the 5-stage SS is reduced (see Fig. 7).

– The CM voltage pulse duty factor γ_{CM} with the $\pm U_d/3$ level for the 5-stage SS ($\lambda = 1$) is 0, because the CM voltage at the 5-stage SS is generated only from levels 0 and $\pm U_d/6$ (see Fig.

Power System Technology
ISSN:1000-3673
Received: 10-01-2024 Revised: 02-02-2024 Accepted: 04-03-2024

11a), while at the 7-stage SS ($\lambda = 0$) and a hybrid SS the $\pm U_d/3$ level is added (see Fig. 11b & c), which inevitably increases in the coefficient γ_{CM} (see Fig. 10d). The maximum CM voltage duty factor for the 7-stage SS reaches 26% when μ is in the region of 0.65, which is explained by the predominance of the operating range of the 7-stage SS and an increase in the switching duration on small basic vectors. For a hybrid SS, the CM voltage pulse duty factor γ_{CM} with the $\pm U_d/3$ level depends on the regulation coefficient λ, which reduces γ_{CM} (Fig. 10d). The degree of reduction of high CM voltage $\pm U_d/3$ is proportional to the switching duration of the 5-stage SS and inversely proportional to the switching duration of the 7-stage SS.

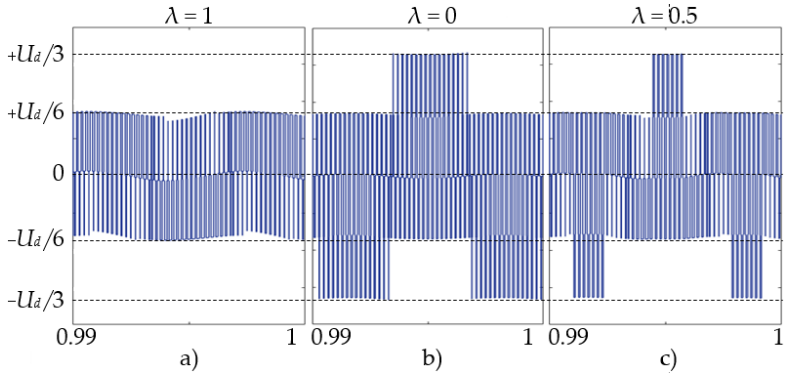

Fig. 11. CM voltage of a 3L NPC VSI at the modulation coefficient μ = 0.75

5.3 Determining the optimal regulation coefficient in a hybrid SS

Taking this into account, the algorithm for a SVPWM with a hybrid SS (see Fig. 8) for any value of the coefficient μ determines the optimal regulation coefficient λ_{OPT} at which the NP voltage deviation $\delta u_{NP.m}$ and the current distortion coefficient THD*i* increase insignificantly, while the number of switchings of power switches n_{SW} and the CM voltage coefficient γ_{CM} decrease significantly compared to the 7-stage SS.

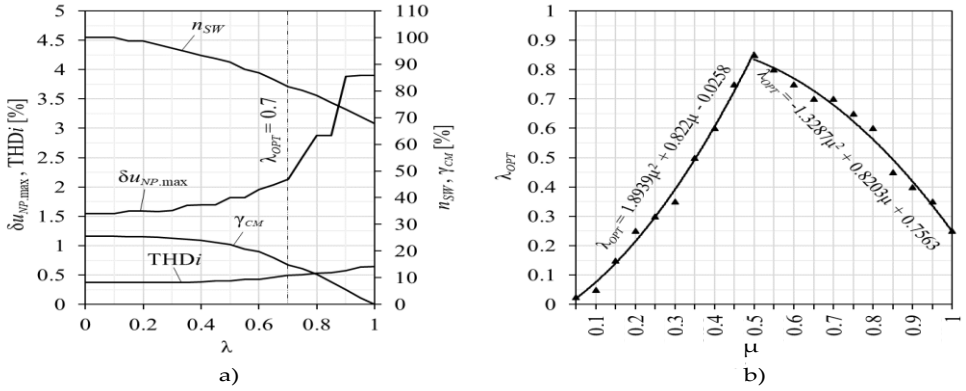

Fig. 12. Dependence graphs: (a) $\mathrm{THD}_i = f(\lambda)$, $\delta u_{NP.\max} = f(\lambda)$, $n_{SW} = f(\lambda)$ and $\gamma_{CM} = f(\lambda)$ at $\mu = 0.7$; and (b) the optimal regulation coefficient $\lambda_{OPT} = f(\mu)$

Power System Technology
ISSN:1000-3673
Received: 10-01-2024 Revised: 02-02-2024 Accepted: 04-03-2024

Figure 12a shows the dependences of $\delta u_{NP.m}$, THDi, n_{SW}, and γ_{CM} constructed at different values of the regulation coefficient λ, for example, at $\mu = 0.7$. The analysis of the dependencies at $\mu = 0.7$ allows the selection of the optimal value of the regulation coefficient λ in a hybrid SS, at which $\delta u_{NP.m}$ and THDi increase insignificantly, while n_{SW} and γ_{CM} decrease by 18% and 10%, respectively. In the same way, we can determine the optimal values of λ_{OPT} for other μ, which are plotted as a dependence $\lambda_{OPT} = f(\mu)$ (see Fig. 12b).

Based on the constructed dependence $\lambda_{OPT} = f(\mu)$, we determined the approximation function of the coefficient λ_{OPT} depending on the modulation coefficient μ:

$$\lambda_{OPT} = \begin{cases} 1{,}8939\mu^2 + 0{,}822\mu - 0{,}0258 & \text{when } \mu \le 0.5; \\ -1{,}3287\mu^2 + 0{,}8203\mu + 0{,}7563 & \text{when } \mu > 0.5. \end{cases} \quad (13)$$

Expression (13) is used in the λ_{OPT} calculator unit (see Fig. 12) to calculate the optimal regulation coefficient λ_{OPT} for any μ values in a hybrid SS.

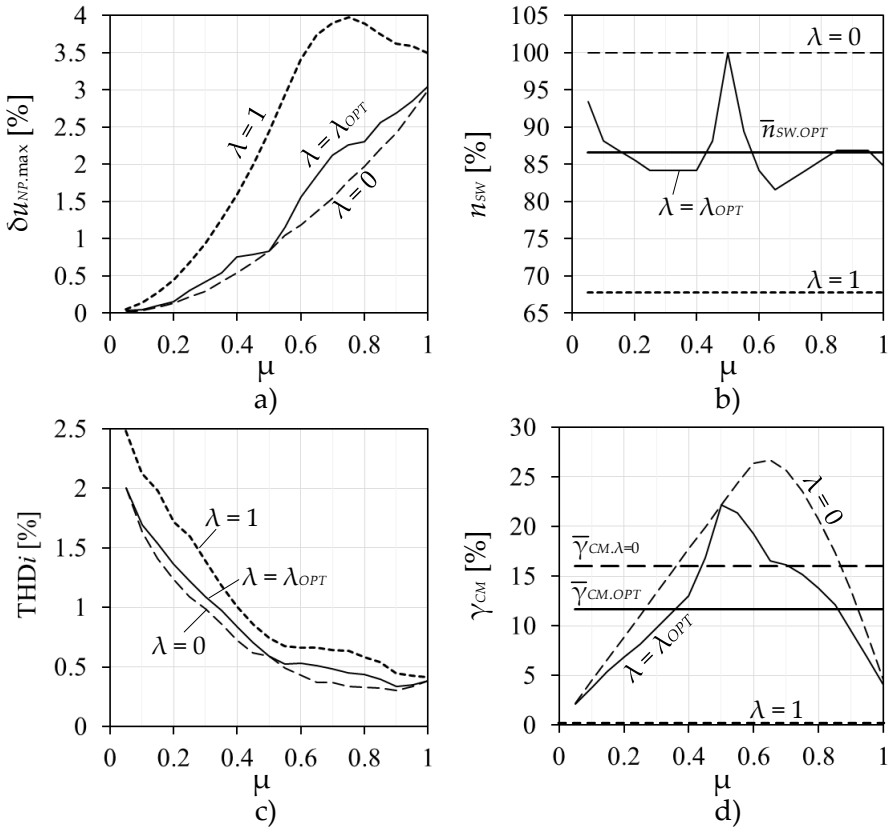

Fig. 13. Dependence graphs: (a) $\delta u_{NP.\max} = f(\mu)$; (b) $n_{SW} = f(\mu)$; (c) THD$i = f(\mu)$; and (d) $\gamma_{CM} = f(\mu)$ at various values of the regulation coefficient $\lambda = 0$, $\lambda = 1$ and $\lambda = \lambda_{OPT}$

Power System Technology
ISSN:1000-3673
Received: 10-01-2024 Revised: 02-02-2024 Accepted: 04-03-2024

To prove the correct choice of the optimal regulation coefficient λ_{OPT}, Figure 13 shows the dependencies of $\delta u_{NP.\max} = f(\mu)$, $n_{SW} = f(\mu)$, $\text{THD}i = f(\mu)$, and $\gamma_{CM} = f(\mu)$ at various values of the regulation coefficient $\lambda = 0$, $\lambda = 1$ and $\lambda = \lambda_{OPT}$.

The analysis of which allowed the following conclusions to be drawn:

– The maximum deviation of the NP voltage $\delta u_{NP.m}$ and the current distortion coefficient THDi compared to the 7-stage SS at $\lambda = \lambda_{OPT}$ do not exceed 0.5% and 0.2%, respectively (see Fig. 13a & c), which is significantly less than for the 5-stage SS.

– The average number of $\overline{n}_{SW.OPT}$ at $\lambda = \lambda_{OPT}$ over the entire range of changes in the modulation coefficient μ decreases by 13.5% compared to the 7-stage SS (see Fig. 13b), which inevitably decreases the switching losses in a 3L VSI with a hybrid SS. The number of switchings of power switches is reduced maximally to 32 % only when the 5-stage SS is used. However, the NP voltage deviation $\delta u_{NP.m}$ here is significantly worse (see Fig. 13a).

– The average pulse duty factor with a high $\pm U_d/3$ level in the CM voltage $\overline{\gamma}_{CM.OPT}$ in the entire range of changes in the modulation coefficient μ at $\lambda = \lambda_{OPT}$ decreases by 4.5% compared to the 7-stage SS (see Fig. 13d). Notably, when only the 5-stage SS is used, there is no high composition with the $\pm U_d/3$ level in the CM voltage and, therefore, $\gamma_{CM} = 0$. Thus, we failed to significantly reduce the CM voltage level in a hybrid SS compared to the 7-stage SS.

6. Experimental results

The generalized composition of the software and hardware for the laboratory equipment is presented in Fig. 14a. The parameters of the laboratory equipment are provided in table 7. IGBT modules of the 3L NPC VSI are controlled by a microprocessor in conjunction with an FPGA. The FPGA includes analog-to-digital converters (ADC) and PWM modules. The microprocessor implements the SVPWM control system with a hybrid SS for managing this inverter. Sets of basic vectors for SVPWM were loaded into the microprocessor's memory in offline mode. Software running on WindowsTM was used to visualize the transient processes of instantaneous values of the converter's electrical signals, as shown in Fig. 14b.

Using the laboratory equipment (Fig. 14), dependencies of the number of power transistor switchings n_{SW} and the maximum error of the NP voltage $\delta u_{NP.\max}$ were recorded with a change in the modulation coefficient μ for the hybrid SS. The research results indicated that the error in experimental data compared to the model for the number of pairs of power switchings does not exceed 1.0%, and for the maximum error of the NP voltage, it is not more than 2%. This discrepancy can be attributed to differences in the PWM frequency and capacitance values of

Power System Technology
ISSN:1000-3673
Received: 10-01-2024 Revised: 02-02-2024 Accepted: 04-03-2024

the DC-link capacitors in the inverter model and experiment. It confirms the reliability of the theoretical research results presented in the article.

Table 7. Technical Data of Laboratory Equipment

IGBT Modules	P924F33 Vincotech; Voltage: 600 V; Rated Current: 30 A; Maximum Switching Frequency: 50 kHz.
Power Supply	Linear Voltage: 380 V; Frequency: 50 Hz.
DC Capacitance	1034 μF (per rack); Maximum Voltage: 450 V.
Current Sensors	LEM HLSR 20-P/SP33; Range: ±20 A; Bandwidth: 450 kHz; Measurement Error: ±0.5%.
Voltage Sensors	Avago ACPL-C87B; Bandwidth: 25 kHz; Measurement Error: ±0.1%.
FPGA	Xilinx XC9536XL-10VQG44C
Microprocessor	TMS320C28346; Clock Speed: 300 MHz; 256 MB NOR Flash Memory, 2 MB RAM, and 300 MIPS.

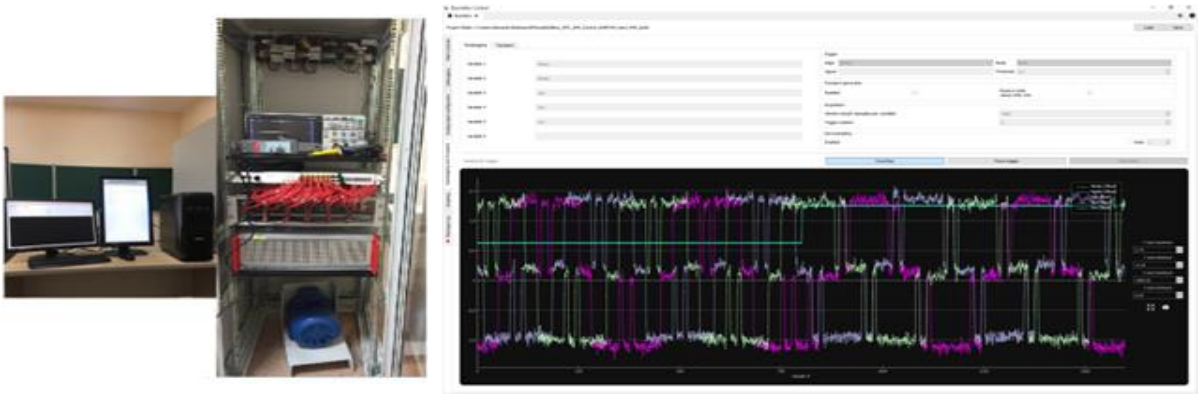

a) b)

Fig. 14. Laboratory equipment for conducting experimental research: an overall view photograph (a) and graphical software BoomBox based on WindowsTM (b).

7. Application of the algorithm for a SVPWM with a hybrid SS

The application of the algorithm for a SVPWM with a hybrid SS is not limited to 3L VSI for high-voltage AC drives but is much broader (Fig. 15). The algorithm can be used in active front ends (AFE) to control converter power switches. AFE are used as a power source for 3L inverters in two-level frequency converters [7]. AFE provide a bidirectional energy flow from the network to the electric motor and in the opposite direction at the desired power factor (most often equal to 1.0 in rectifier mode and minus 1.0 in inverter mode), and with the potential

Power System Technology
ISSN:1000-3673
Received: 10-01-2024 Revised: 02-02-2024 Accepted: 04-03-2024

compensation for reactive power in electrical networks, especially when the electric drive operates at low speeds. AFE are the basis for the construction of grid converters for electricity storage systems based on batteries and supercapacitors [29]. These solutions allow a leveling of the active power curves for an autonomous power source (for example, drilling rigs with diesel generators or gas piston units) and ensure uninterrupted power supply to the main drives and auxiliary mechanisms.

Another major application area of the algorithm, which controls converter power switches, is in devices for improving power quality in power supply systems. They include all types of parallel, serial, and hybrid active filters (AF), as well as network conditioners [30], which are the basis for the construction of flexible alternative current transmission systems (FACT). AF are widely used in power supply systems to compensate for the higher harmonics and reactive power in electrical networks. Power conditioners can also stabilize the voltage level under a load, eliminating low-frequency fluctuations, voltage dips, and surges. Figure 15 shows that the proposed algorithm for a SVPWM with a hybrid SS has major practical applications for constructing powerful converters with a wide range of problem solving.

The authors would like to note that the results of the research can also be applied to power plants in the field of renewable energy. The technical and economic analysis can be carried out according to the calculation models previously developed by the authors.

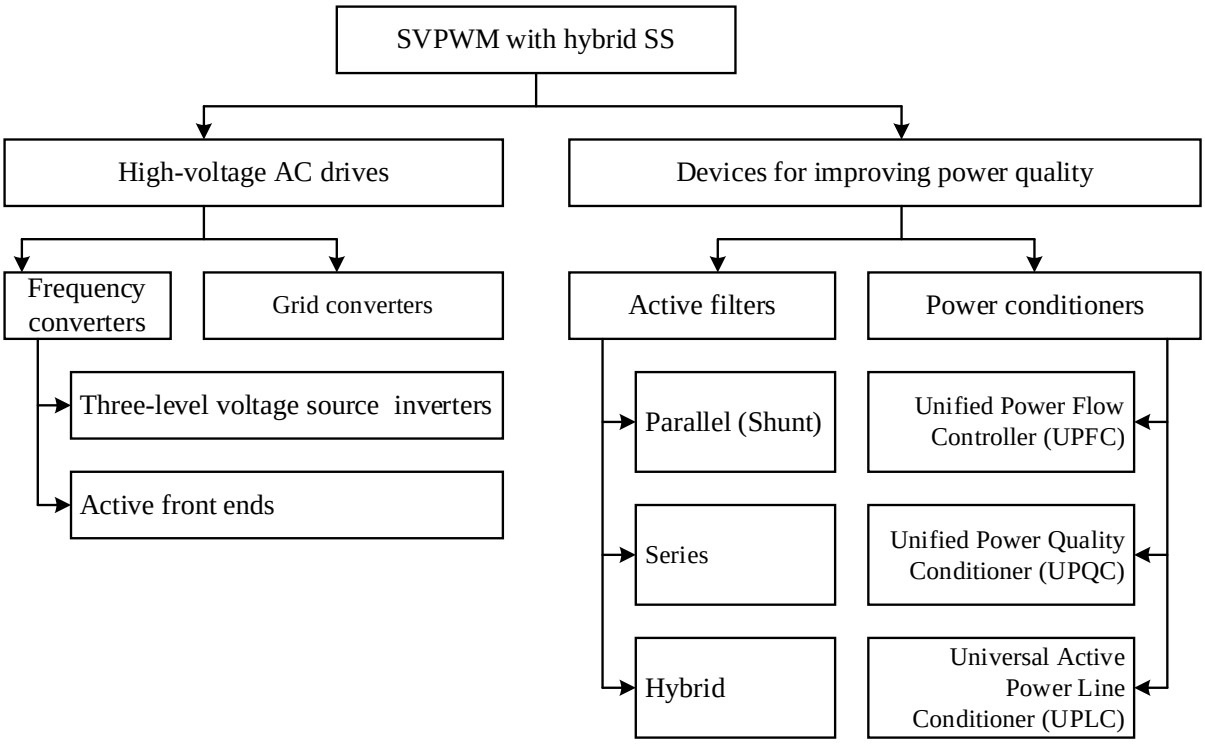

Fig. 15. Applications of the algorithm for a SVPWM with a hybrid SS

Power System Technology
ISSN:1000-3673
Received: 10-01-2024 Revised: 02-02-2024 Accepted: 04-03-2024

8. Conclusion

This paper proposes a new algorithm for a SVPWM with a hybrid SS to control a 3L NPC VSI. Based on the advantages of the 5-stage and 7-stage SS, we developed a hybrid SS to improve the four key parameters in the system: inverter output current quality, NP and CM voltage levels, and switching losses of power switches.

The results of the computer simulation in the *MatLab+Simulink* environment confirmed the effectiveness of the proposed control algorithm and allowed the following basic conclusions to be drawn.

– The use of the SVPWM algorithm only with a 5-stage SS ($\lambda = 1$) solves only two of the four problems: low CM voltage (the absence of high voltage with the $\pm U_d/3$ level, and, therefore, $\gamma_{CM} = 0$) and the smallest number of switchings of power switches, since the position of the spatial voltage vector at the inverter output is formed by four switchings of the basic vectors in each PWM period. However, this results in a high level of the NP voltage imbalance (the maximum error level $\delta u_{NP.m}$ is 4%) and deteriorates the quality of the output current curve (the maximum current distortion coefficient THDi is 2.5%). Consequently, a 5-stage SS is not optimal to control a 3L NPC VSI.

– The use of the SVPWM algorithm only with a 7-stage SS ($\lambda = 0$) provides the best NP balance (the maximum error level $\delta u_{NP.m}$ is 3%) and improves the quality of the output current curve (the maximum current distortion coefficient THDi is 2.0%), but significantly increases the CM voltage level ($\gamma_{CM} = 26\%$) and increases the number of power switch switchings by 33% compared to a 5-stage SS, since the position of the spatial voltage vector at the inverter output is formed by six switchings of the basic vectors at each PWM period. Therefore, a seven-stage SS can neither be considered optimal to control a 3L inverter.

– The proposed algorithm for a SVPWM with a hybrid SS allows the flexible regulation of the four criteria depending on the system operating conditions by changing the regulation coefficient λ. The paper obtained an approximate dependence which allows the optimal regulation coefficient λ_{OPT} to be found for any values of the modulation coefficient μ of the inverter when operating jointly with an active-inductive load. The number of switchings of power switches is reduced by an average of 13.5% while maintaining the NP voltage balance and the quality of the curve at the inverter output at an acceptable level, close to a 7-stage SS (the deviations do not exceed 0.5% and 0.2%, respectively). The average value of the CM voltage coefficient decreased by no more than 4.5% therefore, we failed to achieve a significant reduction in the CM voltage level in the system in the last criterion.

– The laboratory equipment was used to compare experimental data with a computer model for the SVPWM algorithm with a hybrid SS. The research results indicated that the error in

Power System Technology
ISSN:1000-3673
Received: 10-01-2024 Revised: 02-02-2024 Accepted: 04-03-2024

experimental data compared to the model for the number of pairs of power switchings does not exceed 1.0%, and for the maximum error of the NP voltage, it is not more than 2%. This confirms the reliability of the theoretical research results presented in the article.

The implementation of the algorithm for a SVPWM with a hybrid SS is significantly simplified by the use of accurate and reliable advanced microprocessors, which will expand the application area of this algorithm by increasing its efficiency and practical applicability in precision and high-voltage AC electric drives and devices for improving the power quality in power supply systems.

Refrences

[1] Gorozhankin, A.N.; Dudkin, M.M. Algorithms and Control Systems for Electric Drives of Cold Pipe-Rolling Mills. *Russian Electrical Engineering* **2020**, *91*, 440–446. doi: 10.3103/s1068371220070068

[2] Haitham, A.R.; Joachim, H.; Jose, R.; Ge, B. Medium-Voltage Multilevel Converters—State of the Art, Challenges, and Requirements in Industrial Applications. *IEEE Transactions on Industrial Electronics* **2010**, *57*, 2581–2596. doi: 10.1109/TIE.2010.2043039

[3] Klug, R.-D.; Klaassen, N. High power medium voltage drives - innovations, portfolio, trends. *European Conference on Power Electronics and Applications* **2006**, 1–10. doi: 10.1109/EPE.2005.219669

[4] Rodriguez, J.; Lai, J.-S.; Peng, F.Z. Multilevel inverters: a survey of topologies, controls, and applications. *IEEE Transactions on Industrial Electronics* **2002**, *49*, 724–738. doi: 10.1109/TIE.2002.801052

[5] Kushawaha, P.; Rupapara, V.J.; Shah, P.M. Significance of Capacitor Voltage Balancing in Multilevel Inverter. *IEEE International Conference on Innovations in Communication, Computing and Instrumentation (ICCI)* **2019**, 136–142. doi: 10.1109/ICCI46240.2019.9404391

[6] Gupta, H.; Yadav, A.; Maurya, S. Multi carrier PWM for cascade topology of multilevel inverter. *International Conference on Recent Trends on Electronics, Information, Communication & Technology (RTEICT)* **2020**, 328–332. doi: 10.1109/RTEICT49044.2020.9315586

[7] Wu, B; Narimani, M. High-Power Converters and AC Drives Second Edition; Wiley-IEEE Press, 2016; 480 p, ISBN 978-1-119-15606-2.

[8] Nabae, A.; Takahashi, I.; Akagi, H. A new neutral-point-clamped PWM inverter. *IEEE Transactions on Industry Applications* **1981**, *IA-17*, 518–523. doi: 10.1109/TIA.1981.4503992

Power System Technology
ISSN:1000-3673
Received: 10-01-2024 Revised: 02-02-2024 Accepted: 04-03-2024

[9] Mario, S.; Thomas, F.; Johann W.K. Comparative evaluation of advanced three-phase three-level inverter/converter topologies against two-level systems. *IEEE Transactions on Industrial Electronics* **2013**, *60*, 5515–5527. doi: 10.1109/TIE.2012.2233698

[10] Arkan, A.K. PWM control techniques for three phase three level inverter drives. *TELKOMNIKA (Telecommunication, Computing, Electronics and Control)* **2020**, *18*, 516–529. doi: 10.12928/telkomnika.v18i1.12440

[11] Josep, P.; Jordi, Z.; Salvador, C.; Maryam, S.; Dushan, B. A carrier-based PWM strategy with zero-sequence voltage injection for a three-level neutral-point-clamped converter. *IEEE Transactions on Power Electronics* **2012**, *27*, 642-651. doi: 10.1109/TPEL.2010.2050783

[12] Mythili, M.; Kayalvizhi, N. Harmonic minimization in multilevel inverters using selective harmonic elimination PWM technique. *2013 International Conference on Renewable Energy and Sustainable Energy (ICRESE)* **2013**, 70–74. doi: 10.1109/ICRESE.2013.6927790

[13] Sanjiba, K.B.; Nirmal, K.A. SHE PWM technique for three phase three level voltage source inverter. *IEEE International Conference on Power, Control, Signals and Instrumentation Engineering (ICPCSI)* **2017**, 1742–1746. doi: 10.1109/ICPCSI.2017.8392012

[14] Keqing, Q.; Xi, J.; Yuehong, X.; Zuojin, D.; Wendong, C. A SVPWM control strategy for NPC three-level inverter. *IEEE Power Engineering and Automation Conference* **2011**, 256–259. doi: 10.1109/PEAM.2011.6134849

[15] Wei, C.; Haiwei, S.; Xin, G. Synchronized space-vector PWM for three-level VSI with lower harmonic distortion and switching frequency. *IEEE Transactions on Power Electronics* **2016**, *31*, 428–6441. doi: 10.1109/TPEL.2015.2499774

[16] Shishkov, A.N.; Dudkin, M.M.; Le, V.K.; Eremin, N.A. Neutral Point Voltage Balance Based on Space-Vector PWM with Five-Stage Sequence for Three-Level Voltage Inverter. *International Russian Smart Industry Conference (SmartIndustryCon*) **2023**, 586-592. doi: 10.1109/SmartIndustryCon57312.2023.10110815

[17] Luca, D.; Simon, D.R.; Uwe, D.; Johann, W.K. Discontinuous space-vector modulation for three-level PWM rectifiers. *IEEE Transactions on Power Electronics* **2008**, *23*, 530–542. doi: 10.1109/TPEL.2007.915160

[18] Chaturvedi, P.K.; Jain, S., Agarwal, P. Reduced switching loss pulse width modulation technique for three-level diode clamped inverter. IET Power Electronics **2011**, *4*, 393–399. doi: 10.1049/iet-pel.2010.0311

[19] Mohan, M.R.; Hiralal, M.S. Three-dimensional space-vector modulation to reduce common-mode voltage for multilevel inverter. *IEEE Transactions on Industrial Electronics* **2010**, *57*, 2324–2331. doi: 10.1109/TIE.2009.2027247

Power System Technology
ISSN:1000-3673
Received: 10-01-2024 Revised: 02-02-2024 Accepted: 04-03-2024

[20] Tian, K.; Wang, J.; Wu B.; Cheng, Z.; Zargari, N.R. A virtual space vector modulation technique for the reduction of common-mode voltages in both magnitude and third-order. *IEEE Transactions on Power Electronics* **2015**, *31*, 839–848. doi: 10.1109/TPEL.2015.2408812

[21] Shishkov, A.N.; Dudkin, M.M.; Le, V.K.; Eremin, N.A. The Influence of Different Types of Switching Sequences in Space-Vector PWM on Output Characteristics of Three-Level Voltage Inverter. *International Ural Conference on Electrical Power Engineering (UralCon)* **2023**, 690–696. doi: 10.1109/UralCon59258.2023.10291119

[22] Celanovic, N.; Boroyevich, D. A comprehensive study of neutral-point voltage balancing problem in three-level neutral-point-clamped voltage source PWM inverters. *IEEE Transactions on Power Electronics* **2000**, *15* 242-249. doi: 10.1109/63.838096

[23] Zhang, H.; Jouanne, A.V.; Dai, S.; Wallace, A.K., Wang, F. Multilevel inverter modulation schemes to eliminate common-mode voltages. *IEEE Transactions on Industry Applications* **2000**, *36*, 1645–1653. doi: 10.1109/28.887217

[24] Feng, D.W.; Wu, B.; Wei, S.; Xu, D. Space vector modulation for neutral point clamped multilevel inverter with even order harmonic elimination. *Canadian Conference on Electrical and Computer Engineering (IEEE Cat. No.04CH37513)* **2004**, 1471–1475. doi: 10.1109/CCECE.2004.1349682

[25] Xia, C.; Zhang, G.; Yan, Y.; Gu, X.; Shi, T.; He, X. Discontinuous space vector PWM strategy of neutral-point-clamped three-level inverters for output current ripple reduction. *IEEE Transactions on Power Electronics* **2017**, *32*, 5109–5121. doi: 10.1109/TPEL.2016.2611687

[26] Shishkov, A.N.; Dudkin, M.M.; Le, V.K. Influence of switching sequences on the neutral point voltage balance in a three-level voltage source invertor. *Izvestiya MGTU "MAMI"* **2023**, *17*, 195–205. doi: 10.17816/2074-0530-125204

[27] Busquets-Monge, S.; Bordonau, J.; Boroyevich, D.; Somavilla, S. The nearest three virtual space vector PWM - a modulation for the comprehensive neutral-point balancing in the three-level NPC inverter. *IEEE Power Electronics Letters* **2004**, *2*, 11–15. doi: 10.1109/LPEL.2004.828445

[28] Joshi, P.S.; Sheth, C.V. Modelling of grid tied 3-level diode clamped inverter using space vector PWM for PV system. *5th Nirma University International Conference on Engineering (NUiCONE)* **2015**. doi: 10.1109/NUICONE.2015.7449592

[29] Hou, C.C. A multi-carrier PWM for parallel three-phase active front-end converters. *IEEE Energy Conversion Congress and Exposition* **2011**. doi: 10.1109/ECCE.2011.6064324

[30] Akagi, H.; Watanabe, E.H.; Aredes, M. Instantaneous power theory and applications to power conditioning. The power engineering: Handbook; USA: Wiley-IEEE Press; 1st edition, **2007**; 379 p, ISBN-10 0470107618, ISBN-13 978-0470107614.